



HAL
open science

Damage detection on composite beam under transverse impact using the Wave Finite Element method

M. Mallouli, M.A. Ben Souf, O. Bareille, M.N. Ichchou, T. Fakhfakh, M. Haddar

► To cite this version:

M. Mallouli, M.A. Ben Souf, O. Bareille, M.N. Ichchou, T. Fakhfakh, et al.. Damage detection on composite beam under transverse impact using the Wave Finite Element method. *Applied Acoustics*, 2019, 147, pp.23 - 31. 10.1016/j.apacoust.2018.03.022 . hal-03486652

HAL Id: hal-03486652

<https://hal.science/hal-03486652>

Submitted on 20 Dec 2021

HAL is a multi-disciplinary open access archive for the deposit and dissemination of scientific research documents, whether they are published or not. The documents may come from teaching and research institutions in France or abroad, or from public or private research centers.

L'archive ouverte pluridisciplinaire **HAL**, est destinée au dépôt et à la diffusion de documents scientifiques de niveau recherche, publiés ou non, émanant des établissements d'enseignement et de recherche français ou étrangers, des laboratoires publics ou privés.



Distributed under a Creative Commons Attribution - NonCommercial 4.0 International License

Damage detection on composite beam under transverse impact using the Wave Finite Element method

M. Mallouli^{a,b}, M. A. Ben Souf^{a,b,*}, O. Bareille^a, M. N. Ichchou^a, T. Fakhfakh^b, and M. Haddar^b

^a*LTDS, École Centrale Lyon, 36 Avenue Guy de Collongue, F-69134 Ecully Cedex, France*

^b*Laboratoire de Mécanique, Modélisation et Productique, École Nationale d'Ingénieurs de Sfax, Tunisie*

Abstract

In this paper, the Wave Finite Element (WFE) approach based on the finite element model and periodic structure theory, is extended in time domain to study the impact damage behavior of laminated composite structures. The targeted application is the damage detection of laminated E-glass/epoxy beam subjected to a transverse low velocity impact. The proposed strategy consist of a dynamic stress analysis using WFE approach and a damage analysis which is performed using Tsai–Wu quadratic failure and Hashin's failure criteria.

Numerical simulations and comparison with the classical finite element prediction were performed to verify the high accuracy of the present method which provides extremely accurate solutions with much smaller system size and lower computational cost.

Keywords: Impact damage / Laminated composite / Wave propagation / Discrete Fourier Transform (DFT) / Failure criteria / Finite Element analysis.

1. Introduction

Due to high strength to weight and stiffness to weight ratios, composite structures are now increasingly used in different applications, such as

*Corresponding author.

Email address: bensouf.mohamedamine@gmail.com (M. A. Ben Souf)

4 aerospace, automobile and civil engineering. During their service lifetime,
5 they are subjected to a wide range of impact loading. These impacts are
6 sometime caused by accidental event or by scarce operational condition-
7 s. However, they are more sensitive to impact damage than conventional
8 metallic structures due to their anisotropic nature. By design, they in-
9 deed present local structural fragility regarding localized transient (some-
10 times high-energy) forces.

11 Low velocity impact could lead to significant damage [1], in terms of matrix
12 cracks, delamination and eventually fibre breakage for higher impact energies,
13 which are not detectable from visible observation and can cause considerable
14 reduction in the residual strength of the composite. In order to produce an
15 effective design of composite structures and to ensure structural integrity, it
16 becomes crucial to understand the damage mechanism in these structures.

17 For that purpose, experimental and numerical techniques have been de-
18 veloped to help investigating the damage prediction of low velocity impacts.
19 Among them, empirical damage prediction models have been derived from
20 conventional instrumented impact test apparatus [2; 3]. An instrumented
21 drop-weight-testing was used together with several non destructive charac-
22 terization techniques, such as an ultrasonic C-scanning, cross-section frac-
23 tography, an optical microscope and X-ray chamber. These techniques could
24 exhibit some correlation between damage or alteration phenomena which are
25 specific to composite structures and the physical signals captured by sen-
26 sors. At this early stage, the focus was carried on composite laminates. In
27 addition, the main goal was then to establish the limits of these materials
28 in terms of resistance for design purpose in applications, where they were
29 considered as an alternative to traditional homogeneous materials. The cor-
30 responding testing procedures are still used in protocols of qualification for
31 new materials. However, following an impact that created a damage, imper-
32 ceptible from a surface inspection, the characterizing delamination growth
33 under fatigue became soon a subject of attention. Model of damage growth
34 were then associated to the study of impact resulting damages [4; 5].

35 In order to simulate the low-velocity impact and to predict the impact-
36 induced damage in laminated composites, various researchers have deployed
37 the numerical methods which are very efficient because the extent and prop-
38 agation of damage can be more easily detected and controlled with minimum
39 human interaction. Most of the earlier works could found in [6; 7]. Compos-
40 ite materials have been also implementing addition feature for monitoring
41 and control purposes. The monitoring of such composite structure as well

42 as the dynamic control of them raised up the need for reduced model that
43 could capture the overall response without impairing the evaluation of the
44 damage sensitive evolution [8; 9].

45 Within recent years, many authors have studied this subject based on the
46 three-dimensional finite element model to analyze interlaminar stress distri-
47 bution and on the three-dimensional stress-based failure criteria to predict
48 damage [10; 11]. However, finite elements analysis becomes impractically
49 large for high frequencies, leading to an assortment of problems (problems of
50 CPU capacity, lack of accuracy, excessive computation cost and time).

51 An alternative, wave-based, approach to investigate the stress distribution
52 is the Wave Finite Element (WFE) method [12; 13; 14]. This approach
53 is based on the finite element method and periodic structure theory which
54 starts from an FE model of only a typical substructure [15] of the periodic
55 structure, then the mass and stiffness matrices of this substructure are used
56 to formulate an eigenvalue problem whose solutions yields the wave properties
57 (wavenumber, wave modes, group velocity, modal density, etc.).

58 The Wave Finite Element method seems to be so interesting, it provides an
59 efficient way and a large decrease of cost and time for computing the forced
60 responses of systems compared to the conventional finite element method.
61 Accordingly, it has been extensively used in the last few years for the free
62 [16] and forced [17] response of waveguides of different natures, such as beam-
63 like structures [18], laminated beams [19] and plates [16; 20], fluid filled pipes
64 [21; 22], etc.

65 In this paper, a novel numerical technique based on the Wave Finite El-
66 ement (WFE) approach in time domain is proposed to study the impact
67 damage behavior of laminated composite structures. The method consists
68 of a dynamic stress analysis using the WFE method and a failure analysis
69 using Tsai–Wu and Hasshin’s failure criteria. The accuracy of the results
70 predicted by the proposed model is validated by comparing with FEM results
71 for a cantilever composite beam.

72 The paper starts with presenting an overview of the WFE method and the
73 extension of this method in time domain. Tsai–Wu quadratic and Hasshin’s
74 failure criteria are described in Sections 3 and 4 followed by a discussion
75 comparing the proposed model and FEM results. Finally, some general con-
76 clusions to this work are given in Section 5.

77 **2. The Wave Finite Element method**

78 In this section, the WFE method for one-dimensional structures is first
 79 briefly reviewed [12; 23; 24]. Then, the forced response is treated for two
 80 classes of problems, say a single Waveguide and two waveguides coupled
 81 through an excited elastic junction.

82 *2.1. Free wave propagation*

83 The WFE method is based on the finite element model of a typical sub-
 84 structure of length d extracted from the global structural waveguide and
 85 meshed with an equal number of nodes, that means the same number of de-
 86 grees of freedom n , on the left and right sides.

87 Assume that the global system is composed of N identical connected sub-
 88 structures along axis x as shown in Fig. 1.

89

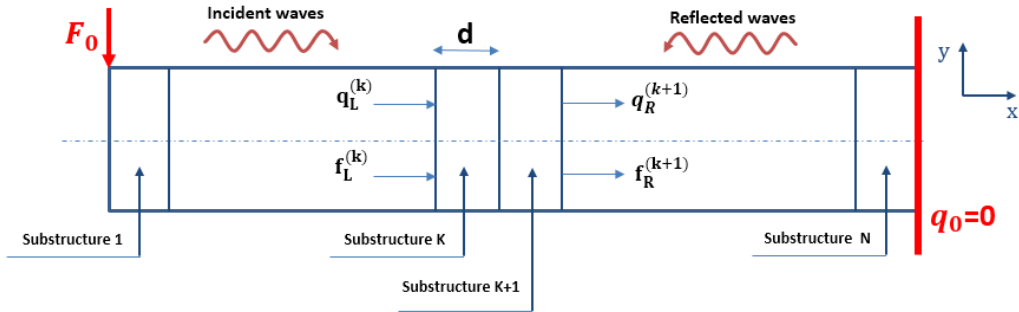


Figure 1: Illustration of a periodic waveguide.

90 The dynamic equilibrium of the substructure is formulated in the fre-
 91 quency domain as:

$$Dq = f \quad (1)$$

92 where q is the vector of the displacement degrees of freedom, f is the applied
 93 forces and D represents the dynamic stiffness matrix of the substructure,
 94 expressed as follows:

$$D = K + j\omega C - \omega^2 M \quad (2)$$

95 where K , C , and M are respectively the stiffness, damping, and mass matri-
 96 ces. The dynamic stiffness operator D can be partitioned and condensed onto

97 its left (L) and right (R) boundaries to give the following matrix equation:

$$\begin{bmatrix} D_{LL} & D_{LR} \\ D_{RL} & D_{RR} \end{bmatrix} \begin{pmatrix} q_L \\ q_R \end{pmatrix} = \begin{pmatrix} f_L \\ f_R \end{pmatrix} \quad (3)$$

98 Assuming there are no external forces applied to the structure, the continu-
 99 ity of displacements and equilibrium of forces at the boundary between two
 100 consecutive substructures k and $k + 1$ yields,

101

$$u_L^{(k+1)} = u_R^{(k)} \quad (4)$$

102 Where the $(2n \times 1)$ state vectors $u_R^T = [(q_R)^T (f_R)^T]$ and $u_L^T = [(q_L)^T (-f_L)^T]$.
 103 the dynamic equilibrium Eq. (1) can be reformulated in this manner:

$$T u_L^{(k)} = u_R^{(k)} = u_L^{(k+1)} \quad (5)$$

104 where T refers to $(2n \times 2n)$ transfer matrix which can be expressed in terms
 105 of the dynamic stiffness matrix [19].

106 Based on Bloch's theorem [25], the propagation constant $\lambda = e^{-jkd}$ relates
 107 the right and left nodal DOFs and forces by:

$$u_R^{(k)} = \lambda u_L^{(k)} \quad (6)$$

108 **Substituting Eq. (6) into Eq. (5) yields an eigenvalue problem:**

$$T \begin{pmatrix} q_L \\ f_L \end{pmatrix} = \lambda \begin{pmatrix} q_L \\ f_L \end{pmatrix} \quad (7)$$

109 The solutions of the eigenvalue problem Eq. (7) are denoted as $\{(\lambda_j, \Phi_j)\}_j$
 110 and are usually called the wave modes traveling along the global structure.
 111 They are split into n incident and n reflected wave modes, corresponding to
 112 positive and negative going waves, respectively (see Fig. 1).

113 The wave mode matrix, denoted Φ , can be partitioned as:

$$\Phi = \begin{bmatrix} \Phi_q^{inc} & \Phi_q^{ref} \\ \Phi_f^{inc} & \Phi_f^{ref} \end{bmatrix} \quad (8)$$

114 where the superscripts *inc* and *ref* refer to as incident and reflected waves
 115 while the subscripts q and f refer to the displacement and force components,
 116 respectively.

117 *2.2. Forced response computation*

118 The strategy for computing the forced response of waveguides has been
 119 proposed in [17; 18]. The vectors of displacements $q^{(k)}$ and forces $f^{(k)}$ at
 120 the substructure boundary k ($k = 1, \dots, N + 1$), along the waveguide can be
 121 written in terms of wave modes $\{\Phi_j\}_j$ and wave amplitudes $\{Q_j\}_j$, as follow:

$$q^{(k)} = \Phi_q^{inc} Q^{inc(k)} + \Phi_q^{ref} Q^{ref(k)}, \quad k = 1, \dots, N + 1 \quad (9)$$

122

$$f^{(k)} = \Phi_f^{inc} Q^{inc(k)} + \Phi_f^{ref} Q^{ref(k)}, \quad k = 1, \dots, N + 1 \quad (10)$$

123 where Q^{inc} and Q^{ref} are respectively the incident and reflected modal am-
 124 plitudes.

125 The spatial distribution those components can be obtained via the following
 126 governing equations:

$$Q^{inc(k)} = \lambda^{k-1} Q^{inc(1)}, \quad k = 1, \dots, N + 1 \quad (11)$$

127

$$Q^{ref(k)} = \lambda^{-(k-1)} Q^{ref(1)}, \quad k = 1, \dots, N + 1 \quad (12)$$

128 with the boundary conditions:

$$Q_{|lim}^{ref} = C Q_{|lim}^{ref} + F \quad (13)$$

129 Here, λ the $(n \times n)$ denotes the diagonal eigenvalue matrix of the incident
 130 modes which is defined as $\lambda = \lambda^{inc} = (\lambda^{ref})^{-1}$, C denotes the $(n \times n)$ diffusion
 131 matrix which provides the reflection and transmission coefficients of the wave
 132 modes across a given boundary and F is $(n \times 1)$ vector whose components
 133 refer to the excitation sources.

134 The Neumann and Dirichlet boundary conditions are write as:

$$\Phi_f^{inc} Q^{inc} + \Phi_f^{ref} Q^{ref} = \pm F_0, \quad (14)$$

135

$$\Phi_q^{inc} Q^{inc} + \Phi_q^{ref} Q^{ref} = q_0. \quad (15)$$

136 In order to reduce the numerical errors [26], the element length must be care-
 137 fully determined when the structure is discretized using FEM.

138 Hence, for the sake of accuracy, the length of substructure should be satisfy-
 139 ing the following condition :

$$d \leq \frac{\lambda_{min}}{2\pi} \quad (16)$$

140 where λ_{min} is the minimal wave length.

141 *2.2.1. Single waveguide*

142 Considering a single waveguide which is split into N identical cells, whose
 143 left and right ends are respectively submitted to prescribed forces and dis-
 144 placements as shown in Fig. 1.

145 In this case, the boundary conditions will be expressed as:

$$\Phi_f^{inc} Q^{inc(1)} + \Phi_f^{ref} Q^{ref(1)} = -F_0 \quad (17)$$

146

$$\Phi_f^{inc} Q^{inc(N+1)} + \Phi_f^{ref} Q^{ref(N+1)} = q_0 \quad (18)$$

147 Using the governing equations Eq. (11) and Eq. (12), we can write:

$$\begin{bmatrix} \Phi_f^{inc} & \Phi_f^{ref} \\ \Phi_q^{inc} \lambda^N & \Phi_q^{ref} \lambda^{-N} \end{bmatrix} \begin{pmatrix} Q^{inc(1)} \\ Q^{ref(1)} \end{pmatrix} = \begin{pmatrix} -F_0 \\ q_0 \end{pmatrix} \quad (19)$$

148 To avoid numerical errors, it will be worth solving Eq. (19) this way:

$$\begin{pmatrix} Q^{inc(1)} \\ Q^{ref(1)} \end{pmatrix} = \begin{bmatrix} I & 0 \\ 0 & \lambda^N \end{bmatrix} \begin{bmatrix} I & (\Phi_f^{inc})^+ \Phi_f^{ref} \lambda^N \\ (\Phi_q^{ref})^+ \Phi_q^{inc} \lambda^N & I \end{bmatrix}^{-1} \times \begin{pmatrix} -(\Phi_f^{inc})^+ F_0 \\ (\Phi_q^{ref})^+ q_0 \end{pmatrix} \quad (20)$$

149 Then, the spatial distribution of the kinematic variables (the vectors of dis-
 150 placements q^k and forces f^k) along the waveguide is obtained by means of
 151 Eqs. (9) and (10).

152 *2.2.2. Two coupled waveguides*

153 The response of two waveguides coupled through an excited elastic cou-
 154 pling element is discussed.

155 It should be noted that, the present formulation is different from that de-
 156 fined in [18]. Where, the coupling element corresponding to impact zone was
 157 subjected to transverse impact.

158 Let's consider two waveguides (1 and 2) and two corresponding substructures
 159 (1 and 2) which are located at the ends of each waveguide and are coupled
 160 with the coupling element, as illustrated in Fig. 2.

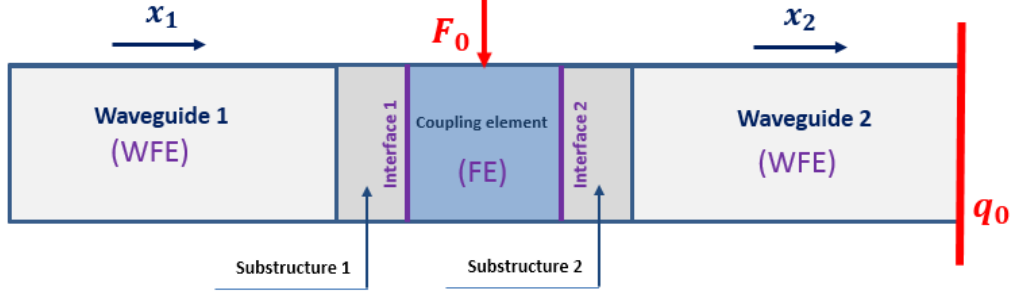


Figure 2: Illustration of two periodic waveguides coupled through an elastic junction.

161 In this case, the matrix C can be partitioned as:

$$C = \begin{bmatrix} C_{11} & C_{12} \\ C_{21} & C_{22} \end{bmatrix} \quad (21)$$

162 where the components of matrices C_{11} and C_{22} denote the reflection coeffi-
 163 cients of the wave modes traveling in waveguides 1 and 2 towards the coupling
 164 junction, while the components of matrices C_{12} and C_{21} denote the transmis-
 165 sion coefficients of these wave modes through the coupling junction.

166 The calculation of these coefficients is presented using a hybrid FE/WFE ap-
 167 proach: the waveguides are modelled using the WFE method and the joint
 168 is modelled using standard FE. It is assumed that the the interfaces guides-
 169 coupling element have compatible meshes and the coupling element is subject
 170 to external forces F_I^c .

171 The dynamical equilibrium of the coupling element can be formulated as
 172 follows:

$$D^c \begin{pmatrix} q_1^c \\ q_I^c \\ q_2^c \end{pmatrix} = \begin{bmatrix} D_{11}^c & D_{1I}^c & D_{12}^c \\ D_{I1}^c & D_{II}^c & D_{I2}^c \\ D_{21}^c & D_{2I}^c & D_{22}^c \end{bmatrix} \begin{pmatrix} q_1^c \\ q_I^c \\ q_2^c \end{pmatrix} = \begin{pmatrix} F_1^c \\ F_I^c \\ F_2^c \end{pmatrix} \quad (22)$$

173 where matrix D^c refers to the complex dynamical stiffness of the coupling ele-
 174 ment, (q_1^c, F_1^c) and (q_2^c, F_2^c) represent the displacements and the forces applied
 175 at the DOFs of the coupling element on interfaces (1 and 2), respectively.
 176 The dynamic condensation of the stiffness matrix of the coupling element

177 into its left and right boundaries, leads to:
 178

$$D^{c*} \begin{pmatrix} q_1^c \\ q_2^c \end{pmatrix} = \begin{pmatrix} F_1^c - D_{1I}^c (D_{II}^c)^{-1} F_I^c \\ F_2^c - D_{2I}^c (D_{II}^c)^{-1} F_I^c \end{pmatrix} \quad (23)$$

179 The couplings conditions of interfaces guides-coupling element are written:

$$\begin{pmatrix} q_1^c \\ q_2^c \end{pmatrix} = \begin{pmatrix} q_R^{(1)} \\ q_L^{(2)} \end{pmatrix}, \quad \begin{pmatrix} F_1^c \\ F_2^c \end{pmatrix} = - \begin{pmatrix} F_R^{(1)} \\ F_L^{(2)} \end{pmatrix} \quad (24)$$

180 Eq.(23)and Eq.(24)give:

$$D^{c*} \begin{pmatrix} q_R^{(1)} \\ q_L^{(2)} \end{pmatrix} = \begin{pmatrix} F_R^{(1)} \\ F_L^{(2)} \end{pmatrix} - \begin{pmatrix} D_{1I}^c (D_{II}^c)^{-1} F_I^c \\ D_{2I}^c (D_{II}^c)^{-1} F_I^c \end{pmatrix} \quad (25)$$

181 q and f vectros are defined as in Section 2.2, thus can be expressed in terms
 182 of the wave amplitudes in the waveguides using Eq. (9) and Eq. (10). Then,
 183 Eq. (25) can be expressed as follows:

$$D^{c*} \left[\Psi_q^{inc} | \Psi_q^{ref} \right] \begin{pmatrix} Q^{inc(1)} \\ Q^{inc(2)} \\ Q^{ref(1)} \\ Q^{ref(2)} \end{pmatrix} = - \left[\Psi_f^{inc} | \Psi_f^{ref} \right] \begin{pmatrix} Q^{inc(1)} \\ Q^{inc(2)} \\ Q^{ref(1)} \\ Q^{ref(2)} \end{pmatrix} - \begin{pmatrix} D_{1I}^c (D_{II}^c)^{-1} F_I^c \\ D_{2I}^c (D_{II}^c)^{-1} F_I^c \end{pmatrix} \quad (26)$$

184 where

$$\begin{aligned} \Psi_q^{inc} &= \begin{bmatrix} \Phi_q^{inc(1)} & 0 \\ 0 & \Phi_q^{inc(2)} \end{bmatrix}, & \Psi_q^{ref} &= \begin{bmatrix} \Phi_q^{ref(1)} & 0 \\ 0 & \Phi_q^{ref(2)} \end{bmatrix} \\ \Psi_f^{inc} &= \begin{bmatrix} \Phi_f^{inc(1)} & 0 \\ 0 & \Phi_f^{inc(2)} \end{bmatrix}, & \Psi_f^{ref} &= \begin{bmatrix} \Phi_f^{ref(1)} & 0 \\ 0 & \Phi_f^{ref(2)} \end{bmatrix} \end{aligned} \quad (27)$$

185 Finally, Eq. (26) can be expressed in this way:

$$[D^{c*} \Psi_q^{inc} + \Psi_f^{inc} | D^{c*} \Psi_q^{ref} + \Psi_f^{ref}] \begin{pmatrix} Q^{inc(1)} \\ Q^{inc(2)} \\ Q^{ref(1)} \\ Q^{ref(2)} \end{pmatrix} = - \begin{pmatrix} D_{1I}^c (D_{II}^c)^{-1} F_I^c \\ D_{2I}^c (D_{II}^c)^{-1} F_I^c \end{pmatrix}. \quad (28)$$

186 The diffusion matrix C is defined such as:

$$\begin{pmatrix} Q^{ref(1)} \\ Q^{ref(2)} \end{pmatrix} = C \begin{pmatrix} Q^{inc(1)} \\ Q^{inc(2)} \end{pmatrix} - [D^{c*} \Psi_q^{ref} + \Psi_f^{ref}]^{-1} \begin{pmatrix} D_{1I}^c (D_{II}^c)^{-1} F_I^c \\ D_{2I}^c (D_{II}^c)^{-1} F_I^c \end{pmatrix} \quad (29)$$

187 where

$$C = -[D^{c*} \Psi_q^{ref} + \Psi_f^{ref}]^{-1} [D^{c*} \Psi_q^{inc} + \Psi_f^{inc}] \quad (30)$$

188 and

$$F = \begin{pmatrix} F_1 \\ F_2 \end{pmatrix} = -[D^{c*}\Psi_q^{ref} + \Psi_f^{ref}]^{-1} \begin{pmatrix} D_{1I}^c(D_{II}^c)^{-1}F_I^c \\ D_{2I}^c(D_{II}^c)^{-1}F_I^c \end{pmatrix}. \quad (31)$$

189 In order to obtain the forced response of the structure, the boundary condi-
190 tions will be expressed as:

191 • For waveguide 1:

$$(\Phi_f^{inc})_1 Q_1^{inc(1)} + (\Phi_f^{ref})_1 Q_1^{ref(1)} = 0 \quad (32)$$

192

$$Q_1^{ref(N_1+1)} = C_{11}Q_1^{inc(N_1+1)} + C_{12}Q_2^{inc(N_2+1)} + F_1 \quad (33)$$

193 • For waveguide 2:

$$Q_2^{ref(N_2+1)} = C_{22}Q_2^{inc(N_2+1)} + C_{21}Q_1^{inc(N_1+1)} + F_2 \quad (34)$$

194

$$(\Phi_q^{inc})_2 Q_2^{inc(1)} + (\Phi_q^{ref})_2 Q_2^{ref(1)} = q_0 \quad (35)$$

195 where N_1 and N_2 denote the numbers of substructures constituting the
196 waveguides 1 and 2, respectively.

197 2.3. Wave Finite Element method in time domain

198 The WFE method enables the calculation of the frequency response of
199 the waveguide and it is extended to obtain also the time response via the
200 Inverse Discrete Fourier Transform (IDFT).

201 The excitation force F_{ext} is sampled into M point signal time $[t_k]_{(k=1..M)}$, then
202 it is transformed into the frequency-domain via Discrete Fourier Transform
203 (DFT).

204 The spectrum of this excitation force \tilde{F}_{ext} can be expressed in the frequency-
205 domain $[\omega_k]_{(k=1..M)}$

$$\tilde{F}_{ext}(\omega_k) = \sum_{m=1}^M F_{ext}(t_m) e^{-jt_m \omega_k} \quad (36)$$

206 At each discrete frequency, this spectrum is used in the WFE approach to
207 calculate the nodal displacement response $\tilde{u}(\omega_m)$.

208 Finally, the data is transformed back to the time-domain by applying an
209 IDFT. The final result is the time history of the displacement at each node.

$$u(t_k) = \frac{1}{M} \sum_{m=1}^M \tilde{u}(\omega_m) e^{-jt_k \omega_m} \quad (37)$$

210 It is to be noted that M , the number of samples should be sufficiently large
211 to avoid numerical problems (Aliasing) and ensure the quality of response in
212 time domain [27].

213 3. Failure Analysis

214 Since impact damage is a very complicated phenomenon, its prediction
215 requires a deep understanding of the basic damage mechanism even in a low
216 velocity impact.

217 Transverse impact initiates critical matrix cracks in a layer within the lami-
218 nate. Delaminations can occur from these matrix cracks immediately along
219 the bottom or upper interface of the cracked layer.

220 In this study, the impact damage analysis follows a two step process. First,
221 Three-dimensional Tsai–Wu failure criterion [28] is used to predict the layer
222 failure in the laminated composite but this quadratic criterion cannot dif-
223 ferentiate between damage modes. Since the propagation of impact-induced
224 damage strongly depends on the damage modes, the Hashin’s [29] criteri-
225 a will be used after the Tsai–Wu failure criteria for determining damage
226 modes (critical matrix cracking, delamination).

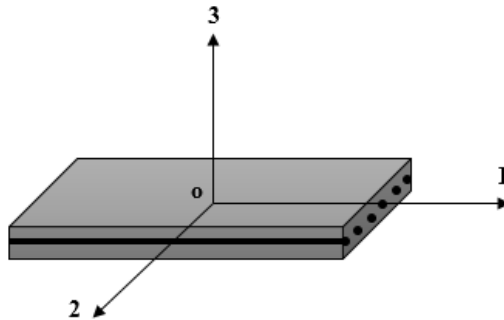


Figure 3: The coordinate system used for the composite laminates.

227 Fig. 3 shows the the coordinate system used to describe the properties
228 of a layer, were the 1 direction is along the fibres and 2 direction normal
229 to the fibres in the laminate plane and 3 direction is through the laminate
230 thickness.

231 *3.1. Tsai–Wu failure criterion*

232 In order to predict accurately the impact damage of entire ply, three-
 233 dimensional Tsai–Wu failure criterion is used. This failure criterion has been
 234 thought as an extension of the Von Mises criterion to a quadratic criterion.
 235 For a three-dimensional stress state, it is given by the equation :

$$F_1\sigma_{11} + F_2\sigma_{22} + F_3\sigma_{33} + F_{11}\sigma_{11}^2 + F_{22}\sigma_{22}^2 + F_{33}\sigma_{33}^2 + F_{44}\sigma_{23}^2 \\ + F_{55}\sigma_{13}^2 + F_{66}\sigma_{12}^2 + 2F_{12}\sigma_{11}\sigma_{22} + 2F_{13}\sigma_{11}\sigma_{33} + 2F_{23}\sigma_{22}\sigma_{33} = I_{TW} \quad (38)$$

236 The following strength parameters account for ply failure:

$$F_1 = \frac{1}{X_t} - \frac{1}{X_c}, \quad F_{12} = -\frac{1}{2\sqrt{X_t X_c Y_t Y_c}} \\ F_2 = \frac{1}{Y_t} - \frac{1}{Y_c}, \quad F_{23} = -\frac{1}{2\sqrt{Y_t Y_c Z_t Z_c}} \\ F_3 = \frac{1}{Z_t} - \frac{1}{Z_c}, \quad F_{13} = -\frac{1}{2\sqrt{X_t X_c Z_t Z_c}} \\ F_{11} = \frac{1}{X_t X_c}, \quad F_{44} = \frac{1}{S_{23}^2} \\ F_{22} = \frac{1}{Y_t Y_c}, \quad F_{55} = \frac{1}{S_{13}^2} \\ F_{33} = \frac{1}{X_t X_c}, \quad F_{66} = \frac{1}{S_{12}^2} \quad (39)$$

237 where :

238 X_t, X_c - tensile and compressive strength in the fibre direction, respectively;
 239 Y_t, Y_c - tensile and compressive strength in the transverse direction, respec-
 240 tively;

241 Z_t, Z_c - tensile and compressive strength in the through-thickness direction,
 242 respectively;

243 S_{12} - shear strength in the fibre and transverse plane;

244 S_{23} - shear strength in the transverse and through-thickness plane;

245 S_{13} - shear strength in the through-thickness and fibre plane.

246

247 *3.2. Hashin's failure criteria*

248 The Hashin's criteria differ slightly from the latter and they allow distin-
 249 guishing between damage modes. Accordingly, two failure criteria, critical

250 matrix cracking criterion and impact-induced delamination criterion, are u-
251 tilized.

252 3.2.1. Critical matrix cracking criterion

253 In order to predict the extent of the critical matrix cracks, Hashin pro-
254 posed a criterion for matrix cracking which it is applied to points in the layers
255 to find the locations of matrix cracks during impact.

256 The matrix failure criterion can be expressed as follows:

$$\left(\frac{\sigma_{22} + \sigma_{33}}{Y_t}\right)^2 + \left(\frac{\sigma_{12}^2 + \sigma_{13}^2}{S_{12}^2}\right) + \left(\frac{\sigma_{23}^2 - \sigma_{22}\sigma_{33}}{S_{23}^2}\right) = I_M. \quad (40)$$

257 3.2.2. Delamination criterion

258 If the initial matrix crack is predicted in a layer of the laminate, a delam-
259 ination can be initiated from this crack.

260 Hashin proposed delamination criterion which it is applied to points in the
261 upper and lower interfaces to determine whether delamination occurs. It can
262 be expressed as:

$$\left(\frac{\sigma_{33}}{Z_t}\right)^2 + \left(\frac{\sigma_{23}}{S_{23}}\right)^2 + \left(\frac{\sigma_{13}}{S_{13}}\right)^2 = I_D. \quad (41)$$

263 The left-hand side of Eq. (39), (40) and (41), I_{TW} , I_M and I_D denote failure
264 index since damage is checked when the index at a point exceeds unity.

265 4. Numerical validations

266 The main use of the numerical application is to predict damage in E-
267 glass/epoxy composite beam subjected to transverse impact. The steps of
268 this analysis are summarized below:

- 269 • Using WFE method in time-domain to calculate the stresses in the
270 global coordinate for each Gaussian point at each element.
- 271 • Calculate the failure index in the Gaussian points by using Tsai–Wu
272 and Hashin’s failure criteria to predict the extent of the impact damage.

273 In order to verify the accuracy of the method used in this study, a three-
274 dimensional dynamic finite element analysis, carried out by using the com-
275 mercial finite element program ANSYS, was performed for calculating the
276 stresses inside the composites during impact.

277 In this section, two examples are presented to verify the accuracy of the

278 approach outlined above. The first is a clamped laminated beam, with rect-
 279 angular cross-section, whose free end is submitted to transverse impact. The
 280 second example is two laminated beams coupled through an excited elastic
 281 junction.

282 *4.1. Cantilevered laminated beam*

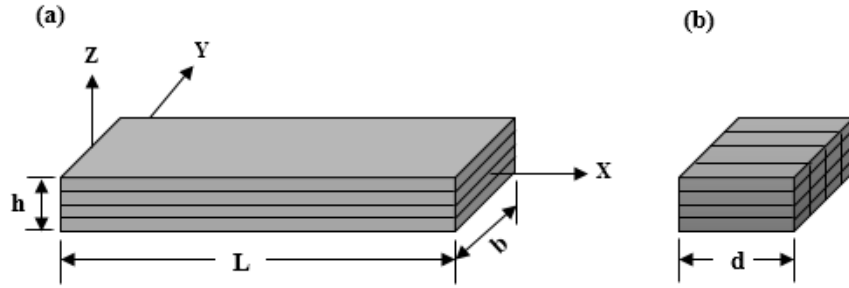


Figure 4: Schematic of the laminated beam: (a) geometry and coordinate systems, (b) schematic of the meshed substructure.

283 A cantilever laminated beam made of E-glass/epoxy is considered for this
 284 study. The beam with dimension: length $L= 0.12$ m, width $b= 0.02$ m and
 285 depth $h= 0.004$ m as presented in Fig. 4. The ply-stacking sequence used
 286 is $[0/45/-45/0]$ degrees and the material properties are listed in Tables. 1
 287 and 2 .

	Symbol (unit)	Value
In-plane longitudinal modulus	$E1$ (GPa)	44.6
In-plane transverse modulus	$E2$ (GPa)	17.0
Out-of-plane transverse modulus	$E3$ (GPa)	16.7
In-plane shear modulus	$G12$ (GPa)	3.49
Out-of-plane shear modulus	$G23$ (GPa)	3.77
Out-of-plane shear modulus	$G13$ (GPa)	3.46
In-plane Poisson's ratio	ν_{12}	0.262
Out-of-plane Poisson's ratio	ν_{23}	0.264
Out-of-plane Poisson's ratio	ν_{13}	0.350
Density	ρ (kg/m^3)	2000

Table 1: Elastic properties of the E-glass/epoxy lamina

	Symbol (unit)	Value
Longitudinal tension	X_t (MPa)	1240
Longitudinal compression	X_c (MPa)	774
Transverse tension	Y_t (MPa)	43.9
Transverse compression	Y_c (MPa)	179
Transverse tension	Z_t (MPa)	31.3
Transverse compression	Z_c (MPa)	185
Ply longitudinal shear	S_{12} (MPa)	55.8
Ply transverse shear	S_{23} (MPa)	45.6
Ply transverse shear	S_{13} (MPa)	54.4

Table 2: Strength properties of the E-glass/epoxy lamina

288 As seen in Fig. 4(b), the waveguide is discretized by means of N identical
289 substructures of length $d = 0.5$ mm. This mesh is supposed to be fine
290 enough to avoid the FE discretization error. Each layer was modelled with
291 four SOLID185 elements which is defined by eight-nodes having three degrees
292 of freedom at each node: translations in the nodal x , y , and z directions.

293

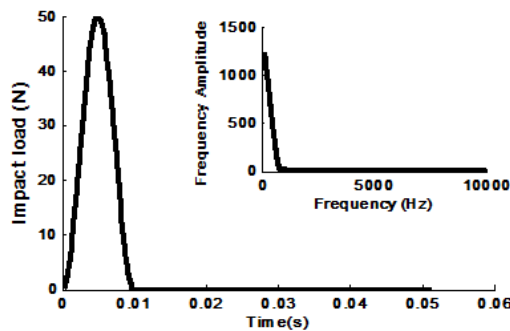


Figure 5: Impact load history and its Frequency spectrum in the inset.

294 An Impact load with peak amplitude 50 N and 10 ms duration as shown
295 in Fig. 5 is considered and the load spectrum is shown in the inset.
296 To ensure the accuracy and validity of the results in the time domain, 8192
297 sampling points M are used for forward and inverse transform of the loading
298 and response, respectively. This spectrum is used in the WFE approach to

299 obtain the frequency response.

300 Subsequently, by applying an Inverse Discrete Fourier Transform (IDFT) to
301 the frequency response (Nodal displacement, strain, stress), the time response
302 can be acquired.

303 This impact load is applied at the left tip of the clamped composite beam
304 in transverse direction. The global system is composed of $N=240$ identical
305 substructures along the x-direction and it contains 18,000 DOFs, while the
306 substructure has 75 DOFs on each side. When the WFE eigenvalue problem
307 of Eq. (8) is solved, 75 incident and 75 reflected wave modes are obtained
308 for computing the forced response of the waveguide. Using the coordinate
309 system shown in Fig. 4, the following points are defined: A($0.02, b/2, h/2$)
310 and B($0.059, b/2, h/2$).

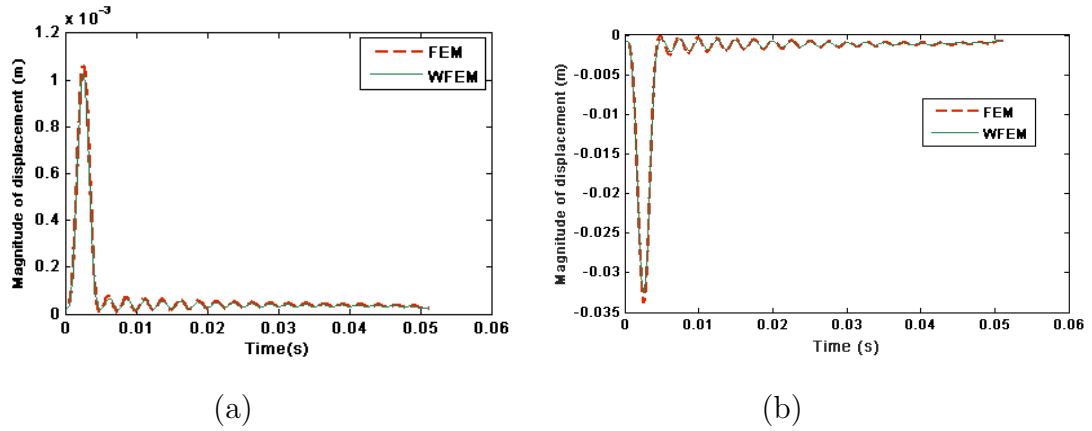


Figure 6: Magnitude of the displacement of the laminated beam at A in the : (a) x-direction,(b) z-direction

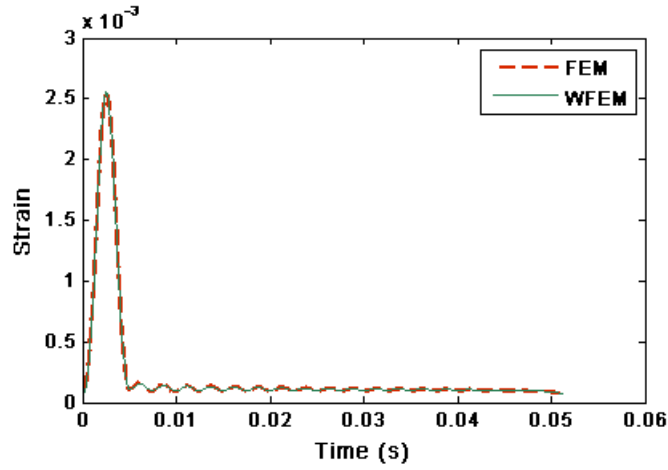


Figure 7: Strain distribution at the last lamina in the x-direction.

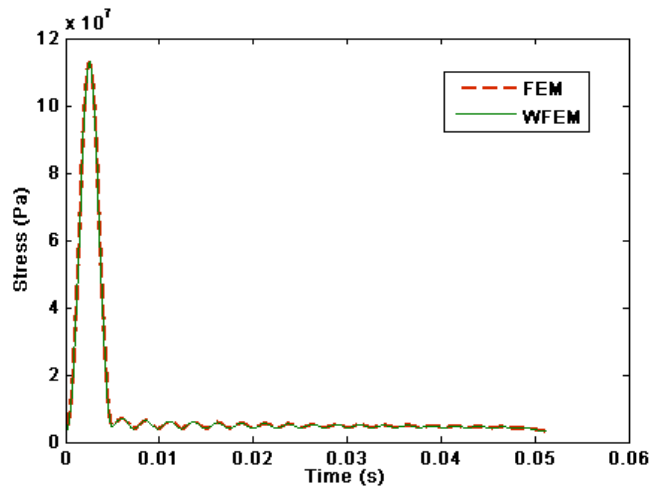


Figure 8: Stress distribution at the last lamina in the x-direction.

311 The forced response of the laminated beam is addressed using the WFE
 312 method in the time domain. The results computed by ANSYS were exported
 313 to MATLAB and plotted to obtain better comparisons with the proposed
 314 method.

315 First, the longitudinal and normal displacement at A in the time domain are
 316 evaluated and compared with a reference solution provided by the FE model

317 as shown respectively in Fig .6(a) and Fig .6(b).A good agreement between
 318 the two results can be observed.

319 These figures also show that the responses obtained by FEM are slightly on
 320 the higher side, which is due the different damping schemes employed by
 321 WFEM and FEM.

322 Next, the strain and stress distribution, in the x-direction on the top surface,
 323 evaluated using the WFE method in time domain are in very good agreement
 324 with the full FEM solutions as shown respectively in Fig .7 and Fig.8. These
 325 figure show that there are very small differences between the results, which
 326 verifies the efficiency of the proposed method in the time domain. These
 327 comparisons with the reference solution obtained by the FE model highlight-
 328 s the validation of the proposed method to estimate the time response of
 329 composite structures subjected to transverse impact.

330 4.2. Two laminated beam coupled with an excited elastic junction

331 4.2.1. Forced Responses

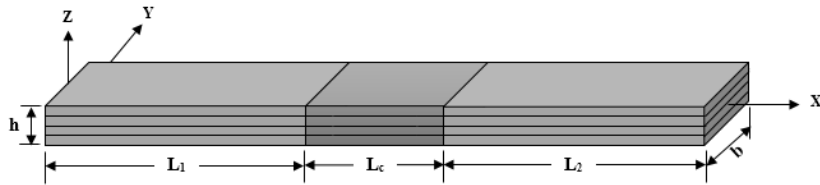


Figure 9: Schematic of the coupled system

332 We consider now the case of two waveguides coupled through an excited
 333 elastic junction depicted in Fig .9. The same impact load defined previously
 334 is applied at the coupling element corresponding to the impact zone. The
 335 other waveguide boundaries, for waveguide 1 and waveguide 2, are respec-
 336 tively free and clamped end. The material of the two waveguides and the
 337 coupling element is E-glass/epoxy with the same parameters as for the lam-
 338 inated beam listed in Tables. 1 and 2.

339 The two waveguides have the same cross-sectional area $b \times h = 0.02m \times$
 340 $0.004m$, while their respective lengths are $L_1 = 0.05m$ and $L_2 = 0.05m$.
 341 These are discretized by means of similar substructures of length $d = 0.5mm$,
 342 so that each of them contains $N_1 = N_2 = 100$ substructures.

343 The length of the coupling element is $L_c = 0.02m$ and its cross-section is

344 similar to those of the connected waveguides.
 345 The SOLID185 elements are used for the discretization of two waveguides
 346 and the elastic junction.
 347 The forced response of the coupled system was computed as shown in Fig.
 348 10 and Fig. 11.
 349 Fig. 10 shows the displacement in the x-, y- and z-directions at B and Fig.
 350 11 shows the history of stress in the x-, y- and z-directions at the centre of
 351 the top surface of the composite beam.
 352 Compared to the reference FE solution when the full coupled system is dis-
 353 cretized, the convergence of the method completely agrees.

354

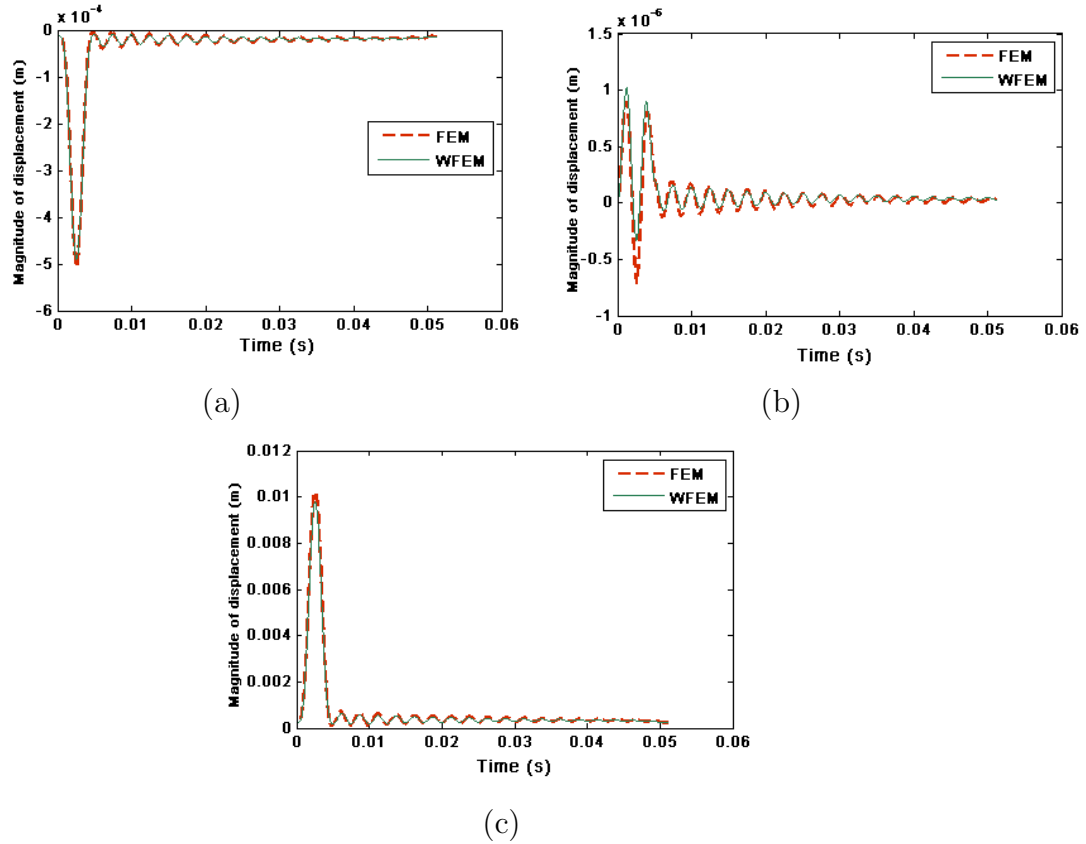


Figure 10: Magnitude of the displacement of the laminated beam at B in the: (a) x-direction, (b) y-direction and (c) z-direction.

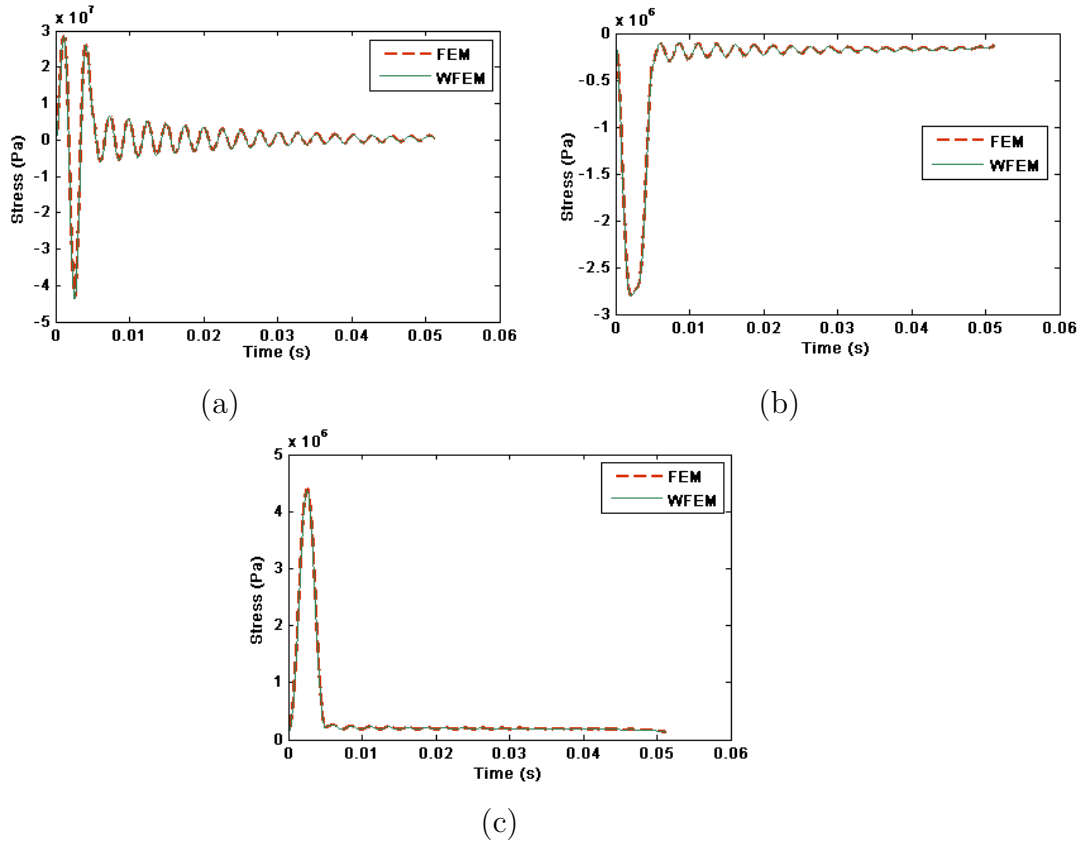


Figure 11: Stress distribution at the last lamina: (a) sigma 1, (b) sigma 2, (c) sigma 3.

355 *4.2.2. Prediction of impact induced damage*

356 In order to investigate the damage initiation behavior of E-glass/epoxy
 357 composite subject to transverse impact, a $[0/45/-45/0]$ laminated beam with
 358 the same properties as the second example defined in the previous section is
 359 considered.

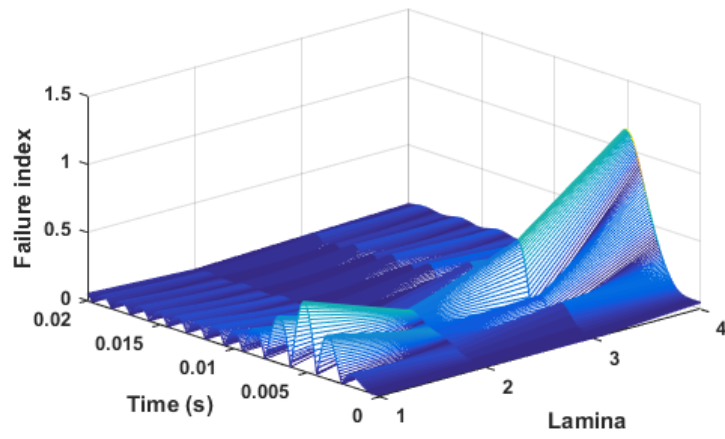
360 Table 3 presents the most critical failure index values of the beam along
 361 the thickness at impact point in different time, obtained through Eq. (38).
 362 Initially, the damage starts in the centre of the top surface corresponding to
 363 the impact position. As the contact force increased, the damage propagated
 364 from the outer layer to the inner layers.

365 As seen in this table, the present formulation predicts failure criteria results
 366 that are in good agreement with results obtained by Ansys program.

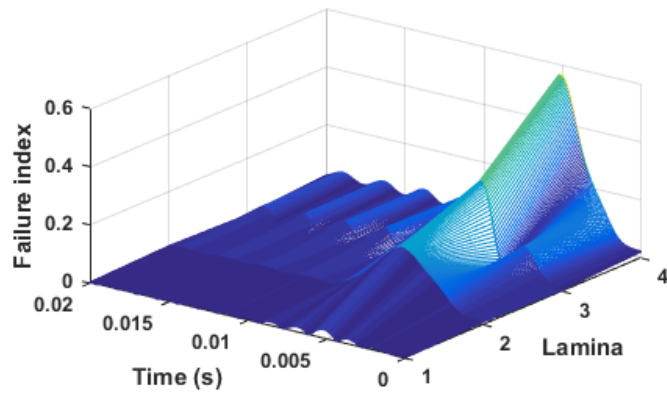
t (ms)	Lam.Nu	Failure index	
		Present Formulation	Ansys
2	1	0.003	0.0025
	2	0.213	0.223
	3	0.2691	0.268
	4	0.213	0.220
3.5	1	0.071	0.075
	2	0.494	0.488
	3	0.040	0.042
	4	0.508	0.521
4.5	1	0.117	0.113
	2	0.7139	0.752
	3	1.281	1.278
	4	1.016	1.015
5	1	0.160	0.163
	2	0.781	0.790
	3	1.584	1.581
	4	1.115	1.113

Table 3: Tsai-Wu index failure.

367 Fig. 12(a) and 12(b) represent the failure indices of matrix cracks for each
368 layer, and delamination failure at the position of the impact point, obtained
369 though Eqs. (40) and (41). It can be observed that all delamination failure
370 indices are less than 1.0, which indicates that the delamination do not occur,
371 and some of the matrix cracks failure indices are however grater than 1.0,
372 indicating that matrix cracks would have occurred in the top layer only.



(a)



(b)

Figure 12: Numerical results of the failure index:(a) failure index of matrix cracks , (b) failure index for delamination

373 5. Conclusion

374 In this paper, the WFE formulation in time domain has been successfully
375 used for computing the forced responses of composite structures. This is the
376 main achievement of the here-reported works. It has been first established
377 and validated on the following test cases: single and coupled system under
378 transverse load.

379 When comparing the WFE representation vs. the full-size conventional FE
380 model, it shows that the WFE solutions are as accurate as the solutions pro-
381 vided by the FE model yet for a considerably lower computational cost.

382 The validation of this formulation is quite important for the prediction of the
383 impact damage evaluation and evolution. Once the stress distribution in the
384 global coordinate at the damage zone are computed, we proceed to calculate
385 firstly the Tsai–Wu index failure to predict the impact damage of entire ply,
386 then the Hashin failure index to identify the damage modes(matrix craks,
387 delamination).

388 Based on these validating and encouraging results, the future work would be
389 the application of the WFE method in time domain to the numerical mod-
390 eling of laminated composites beams with craks and delaminations.

391

392

393 References

- 394 [1] M. O. W. Richardson and M. J. Wisheart. Review of low-velocity impact
395 properties of composite materials. *Composites Part A: Applied Science
396 and Manufacturing*, 27:1123–1131, 1996.
- 397 [2] G. Zhou and G. A. O. Davies. Impact response of thick glass fibre rein-
398 forced polyester laminates. *International Journal of Impact Engineering*,
399 16:357–374, 1995.
- 400 [3] G. Kelly and S. Hallstrom. Strength and failure mechanisms of compos-
401 ite laminates subject to localised transverse loading. *Composite Struc-
402 tures*, 69:301–314, 2005.
- 403 [4] N.H Tai, M.C Yip, and J.L Lin. Effects of low-energy impact on the
404 fatigue behavior of carbon/epoxy composites. *Composites Science and
405 Technology*, 58(1):1 – 8, 1998.

- 406 [5] Milan Mitrovic, H.Thomas Hahn, Greg P. Carman, and Peter Shypryke-
407 vich. Effect of loading parameters on the fatigue behavior of impact
408 damaged composite laminates. *Composites Science and Technology*,
409 59(14):2059 – 2078, 1999.
- 410 [6] S. Abrate, L. Jezequel, and M. Ichchou. Impact on laminated composite
411 materials. *Applied Mechanics Review*, 44:155–190, 1991.
- 412 [7] S.R. Finn and G.S. Springer. Delaminations in composite plates un-
413 der transverse static or impact loads - a model. *Composite Structures*,
414 23:177–190, 1993.
- 415 [8] D. Chronopoulos, M.N. Ichchou, B. Troclet, and O. Bareille. Efficient
416 prediction of the response of layered shells by a dynamic stiffness ap-
417 proach. *Composite Structures*, 97:401–404, 2013.
- 418 [9] Theofanis S. Plagianakos and Evangelos G. Papadopoulos. Low-energy
419 impact response of composite and sandwich composite plates with piezo-
420 electric sensory layers. *International Journal of Solids and Structures*,
421 51(14):2713 – 2727, 2014.
- 422 [10] S. Kumar, B. N. Rao, and B. Pradhan. Effect of impactor parameters
423 and laminate characteristics on impact response and damage in curved
424 composite laminates. *Journal of Reinforced Plastics and Composites*,
425 26:1273–1290., 2007.
- 426 [11] R.K. Luo, E.R. Green, and C.J. Morrison. An approach to evaluate the
427 impact damage initiation and propagation in composite plates. *Com-
428 posites. Part B, Engineering*, 32:513–520, 2010.
- 429 [12] J.-M. Mencik. On the low - and mid frequency forced response of elastic
430 structures using wave finite element with one-dimentional propagation.
431 *Computers and structur*, 88:674–689, 2010.
- 432 [13] D. Duhamel, B.R. Mace, and M.J. Brennan. Finite element analysis of
433 the vibrations of waveguides and periodic structures. *Journal of sound
434 and vibration*, 294:205–220, 2006.
- 435 [14] A. Kessentini, M. Taktak, M.A. Ben Souf, O. Bareille, M.N. Ichchou,
436 and M. Haddar. Computation of the scattering matrix of guided acousti-
437 cal propagation by the wave finite element approach. *Applied Acoustics*,
438 108:92–100, 2016.

- 439 [15] D.J. Mead. A general theory of harmonic wave propagation in linear
440 periodic systems with multiple coupling. *Journal of sound and vibration*,
441 27:235–260, 1973.
- 442 [16] B.R. Mace, D. Duhamel, and M.J. Brennan. Finite element prediction of
443 wave motion in structural waveguides. *Journal of the Acoustical society*
444 *of America*, 117(5):2835–2843, 2005.
- 445 [17] J.M. Mencik. A model reduction strategy for computing the forced
446 response of elastic waveguides using the wave finite element method.
447 *Computer Methods in Applied Mechanics and Engineering*, 229-232:68–
448 86, 2012.
- 449 [18] J.-M. Mencik and M.N. Ichchou. Multi-mode propagation and diffusion
450 in structures through finite elements. *European Journal of Mechanics*
451 *A/Solids*, 24:877–898, 2005.
- 452 [19] J.M. Renno and B.R.Mace. On the forced response of waveguides using
453 the wave and finite element method. *Journal of Sound and Vibration*,
454 329:5474–5488, 2010.
- 455 [20] M.A. Ben Souf, D. Chronopoulos, M. Ichchou, O. Bareille, and M. Had-
456 dar. On the variability of the sound transmission loss of composite panels
457 through a parametric probabilistic approach. *Journal of Computational*
458 *Acoustics*, 24(1), 2016.
- 459 [21] J.-M. Mencik and M.N. Ichchou. Wave finite elements in guided e-
460 lastodynamics with internal fluid. *International Journal of Solids and*
461 *Structures*, 44:2148–2167, 2007.
- 462 [22] E. Manconi, B. Mace, and R. Gaziera. Wave finite element analysis of
463 fluid-filled pipes. *Noise and Vibration: Emerging Methods (NOVEM)*,
464 2009.
- 465 [23] Y. Fan, M. Collet, M. Ichchou, L. Li, O. Bareille, and Z. Dimitrijevic.
466 Energy flow prediction in built-up structures through a hybrid finite
467 element/wave and finite element approach. *Composites Part A: Applied*
468 *Science and Manufacturing*, 66-68:137–158.
- 469 [24] Y. Fan, M. Collet, M. Ichchou, L. Li, O. Bareille, and Z. Dimitrijevic.
470 Enhanced wave and finite element method for wave propagation and

- 471 forced response prediction in periodic piezoelectric structures. *Chinese*
472 *Journal of Aeronautics*, 30(1):75–87, 2017.
- 473 [25] C. Wilox. Theory of bloch waves. *J. Anal Math*, 33(1):146–167, 1978.
- 474 [26] Y. Waki, B.R. Mace, and M.J. Brennan. On numerical issues for the
475 wave/finite element method. *ISVR Technical Memorandum No 964*,
476 2006.
- 477 [27] J.F.Doyle. *Wave propagation in structures: spectral analysis using fast*
478 *discret Fourier transforms*. Springer, second dition edition, 1997.
- 479 [28] S.W. Tsai. Theory of composite design. *Think Composites, Dayton*,
480 1992.
- 481 [29] Z. Hashin. Failure criteria for unidirectional fiber composites. *J Appl*
482 *Mech*, 47:329–334, 1980.